sciendo

***MINERALOGIA**, 49, No 1-4: 99-117 (2018)*
DOI: 10.2478/mipo-2018-0009
www.Mineralogia.pl

MINERALOGICAL SOCIETY OF POLAND
POLSKIE TOWARZYSTWO MINERALOGICZNE

Original paper

Synneusis: does its preservation imply magma mixing?

Bibhuti Gogoi[1], Ashima Saikia[2,*]

[1] *Cotton University, Assam, India*
[2] *University of Delhi, Delhi, India*
** Corresponding author*
e-mail: ashima.saikia@gmail.com

Received: *April 26, 2018*
Received in revised form: *October 17, 2018*
Accepted: *December 18, 2018*
Available online: *January 31, 2019*

Abstract. The Ghansura Felsic Dome (GFD) occurring in the Bathani volcano-sedimentary sequence was intruded by mafic magma during its evolution leading to magma mixing. In addition to the mafic and felsic rocks, a porphyritic intermediate rock occurs in the GFD. The study of this rock may significantly contribute toward understanding the magmatic evolution of the Ghansura dome. The porphyritic rock preserves several textures indicating its hybrid nature, i.e. that it is a product of mafic-felsic magma mixing. Here, we aim to explain the origin of the intermediate rock with the help of textural features and mineral compositions. Monomineralic aggregates or glomerocrysts of plagioclase give the rock its characteristic porphyritic appearance. The fact that the plagioclase crystals constituting the glomerocrysts are joined along prominent euhedral crystal faces suggests the role of synneusis in the formation of the glomerocrysts. The compositions of the glomerocryst plagioclases are similar to those of plagioclases in the mafic rocks. The results from this study indicate that the porphyritic intermediate rock formed by the mixing of a crystal-rich mafic magma and a crystal-poor felsic melt.

Key-words: hybrid rock, glomerocrysts, porphyritic, plagioclase, Bathani volcano-sedimentary sequence

1. Introduction

The current understanding of shallow crustal magma chambers is limited to expelled volcanic products or is based on seismic tomography. These shallow magma reservoirs are often intruded by compositionally distinct magmas leading to magma mixing (DePaolo 1981; Grove et al. 1988; Hawkesworth et al. 2000). Evidence for magma mixing has been reported from many volcanic provinces worldwide (Larsen et al. 1938; Eichelberger 1975; Sakuyama 1981; Luhr, Carmichael 1980; Koyaguchi, 1986). Some of the common lines of

evidence for magma mixing include mafic magmatic enclaves or MME (Eichelberger 1975), chilling or net veining of a more mafic phase by the more felsic phase (Vernon et al. 1988), rapakivi and/or antirapakivi texture, poikilitic crystals of quartz and K-feldspar, titanite ocelli, blade "hydrogenic" biotite, spike zones in plagioclase and boxy cellular morphology of plagioclase crystals, acicular apatite (Hibbard 1991; Baxter, Feely 2002), linear trends in binary diagrams joining the compositions of putative end-members (Castro et al. 1990) and correlations of radiogenic isotopic compositions (Faure 1986). Magma mixing is one of the dominant mechanisms involved in triggering volcanic eruptions. When a new magma intrudes an existing magma chamber, the resulting influx of volatiles and the thermal disequilibrium generated may trigger eruptions (Sparks et al. 1977; Huppert et al. 1982; Sosa-Ceballos et al. 2012). However, the exact mechanisms by which mixing occurs between two disparate magmas remains uncertain. There is a consensus that textural analysis can play a vital role in deciphering the behavior of two disparate magmas during their mixing (Perugini et al. 2003; Martin et al. 2006, Charreteur, Tegner 2013; Gogoi et al. 2017; Gogoi et al. 2018a). Furthermore, textural features preserved in volcanic- and hypovolcanic rocks can significantly contribute to understanding magma-chamber dynamics (Martin et al. 2006, Charreteur, Tegner, 2013; Gogoi et al. 2018b; Gogoi, Saikia 2018).

This paper focuses on the porphyritic intermediate rock of the Ghansura Felsic Dome (GFD) of Chotanagpur Granite Gneiss Complex, eastern India. The porphyritic intermediate rock commonly contains monomineralic aggregates or glomerocrysts of plagioclase. Glomerocrysts are a common yet enigmatic texture in magmatic rocks. This distinct texture reflects the aggregation of crystals of a mineral such as feldspar, quartz or chromite (Schwindinger, Anderson 1989). Glomerocryst formation is commonly attributed to the process of synneusis that is defined as the process of aggregation of crystals, suspended in a melt, along similar prominent crystal faces as they are crystallizing (Vogt 1921; Vance 1969; Schwindinger, Anderson 1989). However, glomerocrysts may also comprise crystals joined along irregular, embayed margins, formed due to resorption of crystals rather than crystallization (Hogan 1993). During resorption, intergranular melt is produced along the grain boundaries which acts as binding material for the partially-resorbed crystals to bind together during slow overgrowth. Such partial dissolution of grains may create a boundary layer melt which subsequently cools and binds the closely-spaced crystals together to form glomerocrysts. Crystal clusters or glomerocrysts have mainly been reported from plutonic settings and their origin has been attributed to a variety of mechanisms. Brown (1956) and Brothers (1964) interpreted the union of crystals in layered gabbroic rocks as due to gravity settling in a crystallizing magma chamber. Murata and Richter (1966) suggested that glomerocrysts form by entrainment of crystal aggregates from a pre-existing cumulate mush. Magmatic turbulence in a crystallizing magma chamber was deemed a major factor in the differential movement of crystals in synneusis by Vance (1969). Stull (1979) inferred that the early-formed crystals floating in a crystallizing magma chamber join by synneusis. Dowty (1980) attributed the origin of synneusis to the hydrodynamic forces associated with flow or gravitational settling and explicitly mentioned the importance of mineral chemistry in understanding the complex process of synneusis. However, detailed work on synneusis involving mineral chemistry has not been carried out to date. In fact, our work appears to be the first to use chemical data from mineral grains

involved in synneusis to understand the origin of the texture. Schwindinger and Anderson (1989) attributed the origin of crystal aggregates to synneusis driven by the hydrodynamic forces associated with crystal settling in a liquid-rich magma. Clague et al. (1995) proposed that olivine displays a synneusis-driven aggregation processes due to rapid settling in low-viscosity primitive liquids. Annexation of smaller mineral grains by larger crystals, followed by grain-boundary migration, was proposed by Marsh (1998). By this process, optically-continuous minerals can be produced as a result of rapid coarsening. Schwindinger (1999) considered crystal aggregates to form during magma flow. Ikeda et al. (2002) considered the minimization of the surface energy of the crystal aggregates to be the driving force for aggregation achieved by an increase in the dihedral angle (θ>60º) corresponding to the interfacial energy ratio at a solid-liquid-solid triple junction. Formation of crystal clusters by remobilization of cumulate mushes in the magma system was proposed as a possible mechanism by (Jerram et al. 2003). Renjith (2014) stressed that the formation of crystal clusters by synneusis is facilitated when crystals are in motion due to dynamically-active convection or turbulence in a crystallizing magma. Magmatic turbulence brought about by magma mixing in a syenite magma chamber was considered as the dominant mechanism leading to the development of crystal clusters in the mixed rocks of the Yelagiri Alkaline Complex of southern India (Renjith et al. 2014).

We have investigated the plagioclase glomerocrysts in the porphyritic intermediate rock of the GFD. The aim was to understand the dynamics of a shallow, crustal, felsic magma chamber involving magma mixing using textural- and mineral chemical analyses of this distinctive magmatic texture.

2. Geological setting and field relationships

The GFD is a small felsic unit occurring in the Bathani volcano-sedimentary sequence, a bimodal volcanic- and volcano-sedimentary suite exposed at the northern edge of Chotanagpur Granite Gneiss Complex, eastern India (Figs 1 and 2a). The sequence extends over a known distance of ca 40 km. The type area is located at Bathani village (24° 59.5' N, 85° 16' E) in the Nalanda district, Bihar, India. The volcano-sedimentary unit is composed of garnet-mica schist, rhyolite, tuff, banded iron formation (BIF), chert and carbonates. The bimodal volcanic sequence comprises rhyolite, andesite, pillow basalt, massive basalt, tuff and mafic pyroclastics. Granites crosscutting the volcanic sequence occur as small hillocks and plutons. Based on primary sedimentary and volcanic structures, it can be established that the volcano-sedimentary sequence is overlain by the bimodal volcanic sequence with no marked break between the two sequences (Saikia et al. 2014).

The GFD is a part of the Bathani sequence that preserves good evidence of magma mixing and mingling (Fig. 2b). A detailed discussion can be found in Gogoi et al. (2018b). In the domain studied, several individual zones are characterized by varying degrees of interaction of the mafic magma with the felsic host as discussed immediately below.

(a) Some mafic zones contain angular felsic clasts (Fig. 3a) indicating that solidification had already begun in the host magma chamber when invading magma disrupted it.

(b) Some other mafic zones contain abundant felsic ocelli with reaction surfaces (Fig. 3b). The felsic ocelli have a definite alignment in the mafic rocks. They have various

shapes, i.e. round, angular, elliptical and elongated. Their sizes vary from ca 1-5 cm across.

(c) A small portion of the Ghansura Dome is occupied by intermingled mafic-felsic rocks (Fig. 3c). A well-defined reaction surface can be seen at mafic-felsic contacts there.

(d) There are some isolated patches in the GFD which are completely felsic (Fig. 3d). These remained isolated from mafic intrusion and are relatively fresh. They represent the closest approximation to the composition of the felsic host prior to the intrusion of the mafic magma.

(e) An intermediate zone is characterized by porphyritic rocks (Figs 3e, 3f). The homogenous nature of these rocks suggests that they formed due to extensive mixing of the two contrasting magmas. Phenocrysts (ca 1-10 mm long) of plagioclase are distinctive as is the presence of abundant rapakivi-textured feldspars (Fig. 3e).

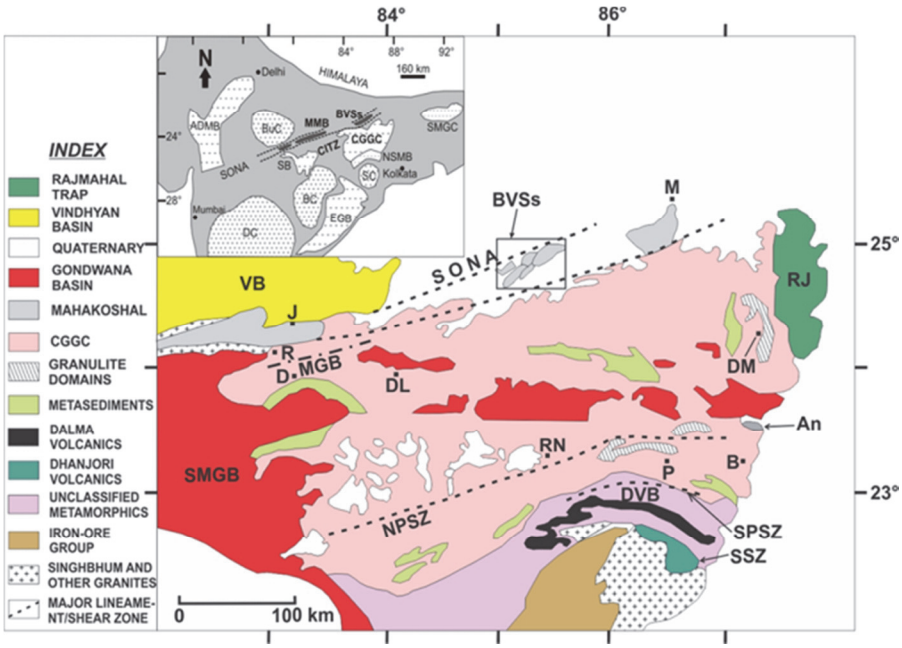

Fig. 1. Geological map of the Chotanagpur Granite Gneiss Complex (modified after Acharyya 2003). Abbreviations: DL- Daltonganj, DM- Dumka, DVB- Dalma Volcanic Belt, D- Dudhi, J- Jirgadandi, MGB- Makrohar Granulite belt, NPSZ- North Purulia Shear Zone, PR- Purulia, RJ- Rajmahal Hills, RN- Ranchi, R- Rihand - Renusagar Area, SMGB- Son Mahanadi Gondwana Basins, SPSZ- South Purulia Shear Zone, SSZ- Singhbhum Shear Zone, SONA- Son Narmada Lineament, M- Munger, VB- Vindhyan Basin, BVSs- Bathani volcano-sedimentary sequence, An- Anorthosite, B- Bankura. The inset shows location of the Chotanagpur Granite Gneiss Complex (CGGC) along with other Proterozoic mobile belts of India including Central India Tectonic Zone (CITZ), North Singhbhum Mobile Belt (NSMB), Eastern Ghats Belt (EGB), Aravalli Delhi Mobile Belt (ADMB) and Shillong Meghalaya Gneissic Complex (SMGC). Four Archean cratonic nuclei of India, namely Bastar (BC), Bundelkhand (BuC), Singhbhum (SC) and Dharwar (KC) are also shown (modified after Chatterjee, Ghosh 2011)..

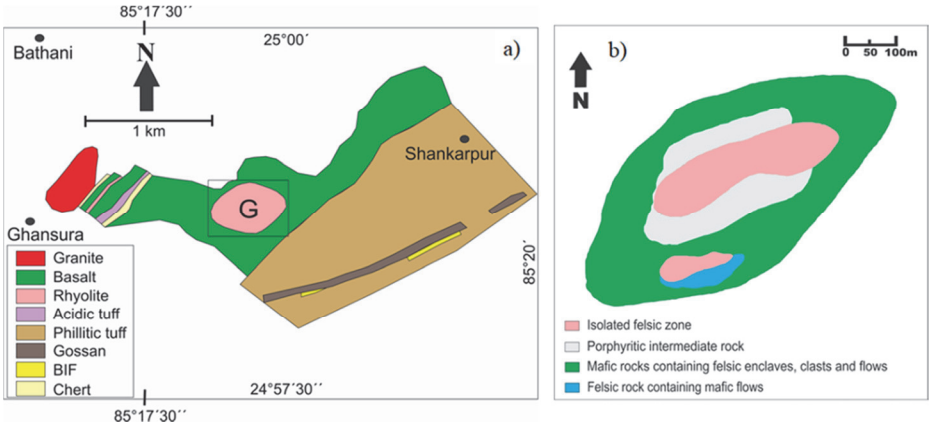

Fig. 2. (a) Geological map of the Bathani volcano-sedimentary sequence (modified after Ahmad, and Paul 2013). The Ghansura Felsic Dome is marked as G (b) Simplified geological map of the Ghansura Felsic Dome.

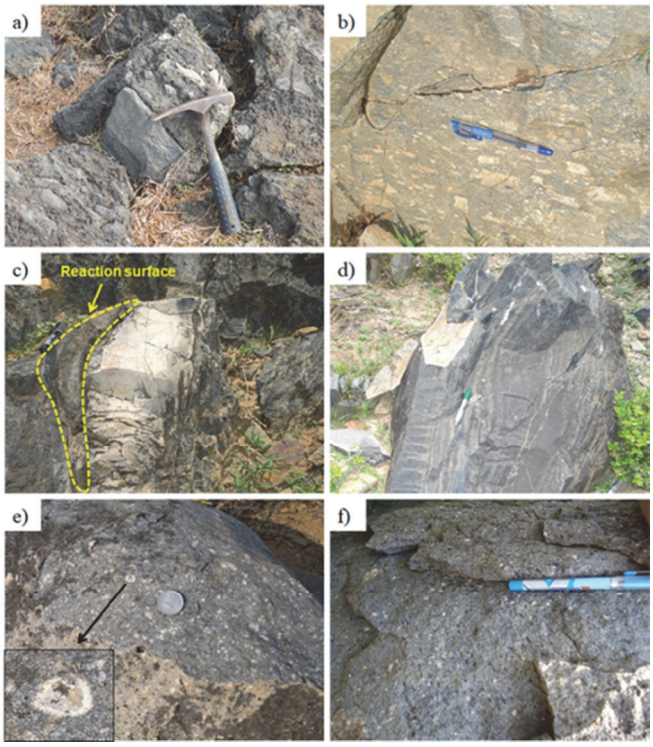

Fig. 3. Field photographs displaying (a) felsic clasts embedded in mafic rock (b) felsic microgranular enclaves or felsic ocelli within mafic rock (c) intermingled mafic and felsic rock, in which, reaction surfaces can be seen at the mafic-felsic contacts (d) isolated felsic rock representing rhyolite (e) porphyritic intermediate rock containing rapakivi-type feldspars (inset shows a magnified feldspar crystal) (f) porphyritic intermediate rock displaying abundant feldspar phenocrysts.

3. Petrography

The rocks of the GFD may be broadly classified into (1) mafic-, (2) felsic- and (3) porphyritic intermediate rock. As the main objective of the present work is to understand the genesis of glomerocrysts in the porphyritic intermediate rock, the petrography of other hybrid rocks from the dome is not discussed.

3.1. Mafic rocks

The mafic rocks consist of augite, plagioclase and Ti-Fe oxide as major phases, and amphibole and biotite as accessory phases. Phenocrysts of augite give the rock a porphyritic texture (Fig. 4a). Most of the plagioclase laths are partially or completely enclosed within augite in ophitic- and sub-ophitic textures.

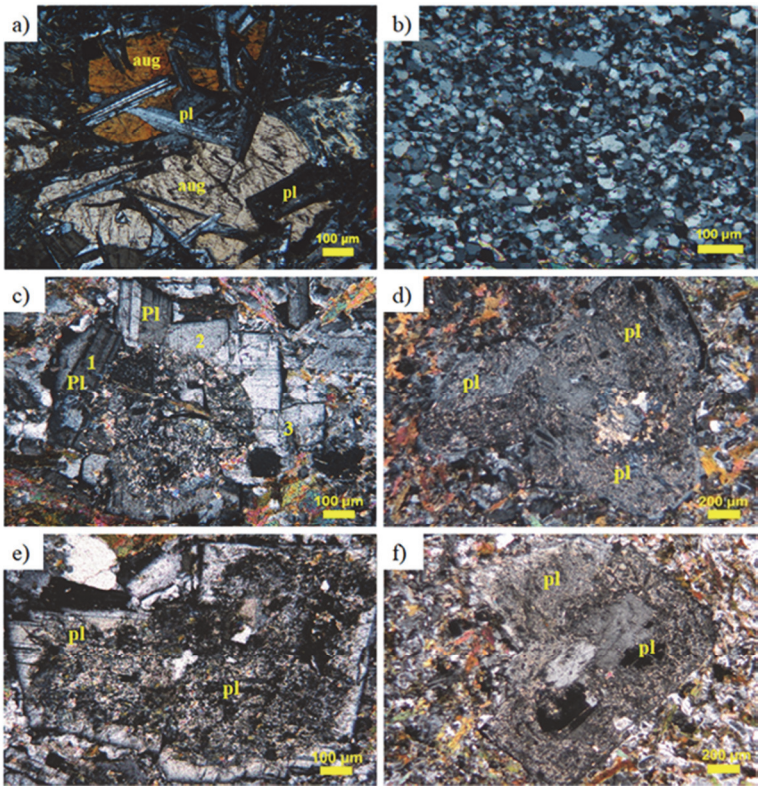

Fig. 4. Photomicrographs displaying (a) ophitic texture in the mafic rock showing plagioclase laths engulfed in augite grains (b) CPL view of the rhyolite (c-f) plagioclase grains involved in synneusis in the porphyritic intermediate rock.

3.2. Felsic rocks

The felsic rocks are fine grained with the mineral grains mostly ranging from subhedral to anhedral in shape (Fig. 4b). They generally consist of quartz, K-feldspar, muscovite and ilmenite.

3.3. Porphyritic intermediate rock

In this rock, phenocrysts of plagioclase lie in a fine to medium grained matrix of quartz, plagioclase, K-feldspar, biotite, calcite, apatite and ilmenite. Quartz ocelli, rapakivi- and anti-rapakivi feldspars, feldspars with dissolved cores and undissolved rims, oscillatory zoning in plagioclase and acicular apatite are all evident.

The aggregation of smaller plagioclase grains into crystal clusters is a striking petrographic feature of this rock (Fig. 4c-f). The crystals forming these clusters have undergone mutual attachment to form larger crystals of plagioclase. The degree of coalescence varies significantly between the plagioclase grains involved. In some cases, the crystals aggregated with their grain boundaries intact (Fig. 4c) whereas, in others, grain boundaries dissolved completely to form a larger plagioclase grain (Fig. 4f). Oscillatory- or other zoning patterns are not observed in the plagioclase crystals in the clusters.

5. Analytical method

Mineral chemical analyses were performed using a CAMECA SX 100 electron microprobe at the Electron Microprobe Analyzer Laboratory, Geological Survey of India, Faridabad (India). The data were obtained using an acceleration voltage of 15 kV, a beam current of 10 nA and a beam diameter of ca 1 μm. Standards used include Wollastonite for Si and Ca, Periclase for Mg, Rhodonite for Mn, Albite for Na, Corundum for Al, Hematite for Fe, Orthoclase for K, Apatite for P, metallic Cr and Ti for Cr and Ti, Halite for Cl, Metallic Zn for Zn, Fluorite for F and Barite for Ba. The PAP correction was applied to the data (Pouchou, Pichoir 1987).

6. Mineral chemistry

Mineral chemical analyses were carried out on plagioclase to understand the genesis of the synneusis texture in the porphyritic intermediate rock. The focus was on plagioclase as it is considered an important phase in tracing magma mixing. Plagioclase forms at a wide range of magma compositions and thermal conditions and does not equilibrate during mafic-felsic magma interactions, valuable information about magma-mixing processes are preserved (Pietranik, Koepke 2009). Plagioclase is present in the mafic- and porphyritic intermediate rocks of the GFD, but not in the felsic rocks.

Analyses were carried out at 13 points in three plagioclase grains in the mafic end-member. The data include core-rim analyses from individual plagioclase grains given in Table 1. Plagioclase compositions plot in the fields of andesine, labradorite and bytownite (Fig. 5a). An contents vary from An_{48} to An_{75}.The plagioclase grains show reverse zoning with Ca-poor cores (An_{48-68}) relative to rims (An_{65-73}).

TABLE 1

Representative electron microprobe analyses of plagioclase feldspar from the mafic end-member of GFD

	Grain 1				**Grain 2**					**Grain 3**			
Location	**Core**			**Rim**	**Core**				**Rim**	**Core**			**Rim**
SiO_2	50.09	48.02	47.97	49.07	54.68	49.15	49.82	49.82	51.34	52.34	50.14	49.45	49.51
TiO_2	0.02	0.00	0.05	0.00	0.01	0.00	0.00	0.09	0.11	0.00	0.00	0.02	0.09
Al_2O_3	31.07	31.91	32.54	32.06	29.42	35.25	31.22	31.02	30.97	27.95	30.15	30.50	30.53
FeO	0.39	0.28	0.28	0.18	0.31	0.81	0.64	0.52	0.24	0.69	0.65	0.80	0.95
MnO	0.00	0.00	0.00	0.06	0.00	0.00	0.00	0.03	0.02	0.01	0.00	0.04	0.00
MgO	0.04	0.08	0.05	0.00	0.05	0.16	0.13	0.13	0.04	0.08	0.15	0.12	0.08
CaO	13.88	15.30	15.51	15.09	9.66	12.46	13.91	14.19	13.51	11.88	13.79	14.38	14.40
Na_2O	3.64	2.79	2.86	3.13	5.68	3.65	3.37	3.44	3.97	4.88	3.79	3.27	3.53
K_2O	0.09	0.11	0.05	0.02	0.16	0.06	0.10	0.07	0.04	0.15	0.16	0.15	0.24
Cl	0.02	0.02	0.01	0.00	0.01	0.02	0.00	0.02	0.00	0.00	0.00	0.00	0.00
F	0.00	0.00	0.06	0.00	0.08	0.19	0.00	0.02	0.00	0.00	0.08	0.00	0.00
BaO	0.00	0.00	0.20	0.00	0.07	0.00	0.01	0.00	0.22	0.14	0.10	0.00	0.26
Total	99.24	98.50	99.57	99.60	100.12	101.74	99.20	99.34	100.45	98.12	99.02	98.72	99.59
Calculation based on 8 O													
Si	2.30	2.23	2.21	2.25	2.46	2.20	2.29	2.29	2.33	2.43	2.32	2.29	2.29
Ti	0.00	0.00	0.00	0.00	0.00	0.00	0.00	0.00	0.00	0.00	0.00	0.00	0.00
Al	1.68	1.75	1.77	1.74	1.56	1.86	1.69	1.68	1.66	1.53	1.64	1.67	1.66
Fe	0.02	0.01	0.01	0.01	0.01	0.03	0.02	0.02	0.01	0.03	0.03	0.03	0.04
Mn	0.00	0.00	0.00	0.00	0.00	0.00	0.00	0.00	0.00	0.00	0.00	0.00	0.00
Mg	0.00	0.01	0.00	0.00	0.00	0.01	0.01	0.01	0.00	0.01	0.01	0.01	0.01

Ca	0.68	0.76	0.77	0.74	0.47	0.60	0.69	0.70	0.66	0.59	0.68	0.71	0.71
Na	0.32	0.25	0.26	0.28	0.50	0.32	0.30	0.31	0.35	0.44	0.34	0.29	0.32
K	0.01	0.01	0.00	0.00	0.01	0.00	0.01	0.00	0.00	0.01	0.01	0.01	0.01
Cl	0.00	0.00	0.00	0.00	0.00	0.00	0.00	0.00	0.00	0.00	0.00	0.00	0.00
F	0.00	0.00	0.01	0.00	0.01	0.03	0.00	0.00	0.00	0.00	0.01	0.00	0.00
Ba	0.00	0.00	0.00	0.00	0.00	0.00	0.00	0.00	0.00	0.00	0.00	0.00	0.00
Total	5.02	5.02	5.03	5.02	5.01	5.04	5.01	5.02	5.01	5.03	5.04	5.02	5.04
An(%)	67.48	74.71	74.79	72.65	47.98	65.10	69.13	69.23	65.16	56.87	66.19	70.23	68.32
Ab(%)	32.01	24.64	24.91	27.25	51.09	34.51	30.28	30.38	34.62	42.30	32.89	28.90	30.34
Or(%)	0.50	0.65	0.30	0.10	0.93	0.39	0.59	0.40	0.22	0.83	0.93	0.87	1.34

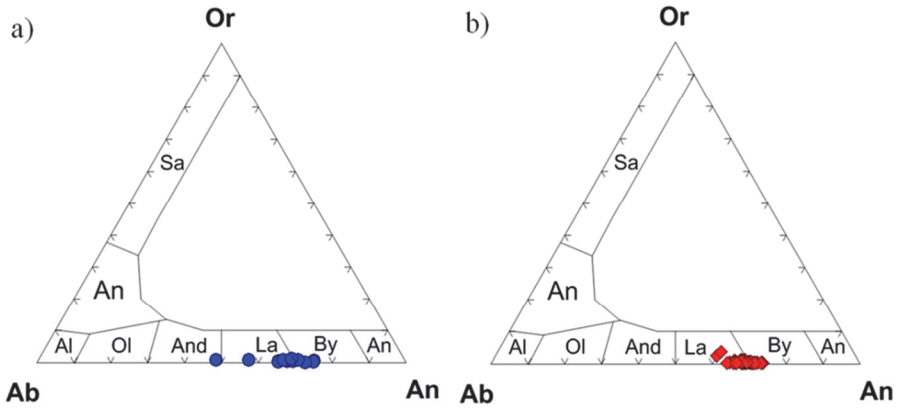

Fig. 5. Nomenclature of plagioclase occurring (a) in the mafic rock (b) in the porphyritic intermediate rock. The plagioclase grains whose compositions were determined are marked in Fig. 4.

Analyses were carried out at 54 points on plagioclase grains occurring in a crystal cluster in the porphyritic intermediate rock. The data include core-rim analyses of individual plagioclase grains. Representative data are provided in Table 2. The compositions of plagioclase from the hybrid product plot in the compositional range of bytownite and labradorite (Fig. 5b). An contents vary between An_{60} and $An_{74.}$ Plagioclase crystals in the crystal cluster show no clear zoning pattern; their compositions are nearly uniform from cores ($An_{69\text{-}71}$) to rims ($An_{66\text{- data}70}$).

Compositions of plagioclase from the mafic end-member and from the porphyritic intermediate rock are plotted to show variations of K_2O, TiO_2, BaO and FeO as a function of anorthite content (Fig. 6a-d). In the variation diagrams, there are substantial similarities between the plagioclase compositions of the mafic rocks and the porphyritic intermediate rocks, excepting FeO which shows slightly higher FeO concentrations in plagioclase for the mafic rocks at similar An contents.

7. Discussion

The Ghansura dome is a small felsic domain that was intruded by mafic magma during its genesis. Various hybridized zones occur which include mafic rocks containing felsic clasts and felsic ocelli (Fig. 3a and b), intermingled mafic-felsic rocks (Fig. 3c) and porphyritic intermediate rock (Fig. 3e and f). From field observations, the hybrid zones appear to have formed due to varying degrees of interaction between invading mafic magma and felsic host. Pure end-member mafic- and felsic rocks not affected by magma mixing and mingling also occur in the area. All these rock types occur together in the GFD is a random distribution pattern. The occurrence of felsic clasts and ocelli within mafic rocks suggests that the felsic magma chamber was partly solidified when mafic magma intruded. The intermingled mafic-felsic rocks suggest mingling of mafic- and felsic magmas in which signatures of both magmas can be traced. In contrast, the porphyritic intermediate rock appears to be a homogenous product in which signatures of the parental

TABLE 2

Representative electron microprobe analyses of plagioclase feldspar involved in synneusis from the porphyritic intermediate rock.

Grain 1																	
Location	**Core**																**Rim**
SiO_2	50.70	53.36	50.70	51.30	50.71	51.74	51.65	51.14	50.42	51.60	51.11	51.59	50.03	50.80	51.91	49.11	50.79
TiO_2	0.00	0.10	0.00	0.00	0.09	0.12	0.00	0.08	0.00	0.00	0.04	0.09	0.16	0.00	0.09	0.00	0.00
Al_2O_3	31.14	29.17	31.04	30.58	30.55	30.87	30.54	30.59	31.27	30.11	29.74	30.48	31.83	30.63	30.51	32.03	31.28
FeO	0.45	0.28	0.29	0.37	0.27	0.26	0.25	0.27	0.45	0.24	0.37	0.21	0.34	0.40	0.46	0.41	0.35
MnO	0.03	0.00	0.03	0.00	0.00	0.03	0.05	0.00	0.07	0.00	0.04	0.00	0.02	0.03	0.00	0.02	0.01
MgO	0.00	0.00	0.00	0.00	0.00	0.00	0.00	0.00	0.00	0.00	0.00	0.00	0.00	0.00	0.00	0.00	0.00
CaO	14.27	12.23	14.10	14.05	12.10	14.17	13.77	13.67	14.83	13.33	14.22	13.63	15.17	13.75	13.47	13.84	14.39
Na_2O	3.50	4.25	3.55	3.61	3.94	3.56	3.55	3.82	3.16	4.02	3.31	3.82	2.99	3.66	3.79	3.85	3.28
K_2O	0.06	0.41	0.06	0.03	0.60	0.05	0.11	0.05	0.09	0.06	0.08	0.08	0.04	0.13	0.17	0.11	0.09
Cl	0.00	0.00	0.00	0.00	0.00	0.02	0.00	0.00	0.01	0.00	0.00	0.01	0.00	0.01	0.00	0.00	0.02
F	0.21	0.00	0.08	0.00	0.00	0.05	0.08	0.00	0.10	0.00	0.00	0.00	0.01	0.14	0.02	0.14	0.11
BaO	0.21	0.32	0.00	0.00	0.01	0.00	0.29	0.34	0.00	0.00	0.00	0.07	0.00	0.17	0.00	0.01	0.21
Total	100.56	100.11	99.85	99.94	98.26	100.86	100.29	99.96	100.41	99.36	98.90	99.97	100.57	99.72	100.42	99.51	100.53
Calculation based on 8 O																	
Si	2.30	2.42	2.31	2.34	2.35	2.33	2.34	2.33	2.29	2.36	2.35	2.35	2.27	2.32	2.35	2.25	2.30
Ti	0.00	0.00	0.00	0.00	0.00	0.00	0.00	0.00	0.00	0.00	0.00	0.00	0.01	0.00	0.00	0.00	0.00
Al	1.67	1.56	1.67	1.64	1.67	1.64	1.63	1.65	1.68	1.62	1.61	1.63	1.70	1.65	1.63	1.73	1.67
Fe	0.02	0.01	0.01	0.01	0.01	0.01	0.01	0.01	0.02	0.01	0.01	0.01	0.01	0.02	0.02	0.02	0.01
Mn	0.00	0.00	0.00	0.00	0.00	0.00	0.00	0.00	0.00	0.00	0.00	0.00	0.00	0.00	0.00	0.00	0.00
Mg	0.00	0.00	0.00	0.00	0.00	0.00	0.00	0.00	0.00	0.00	0.00	0.00	0.00	0.00	0.00	0.00	0.00
Ca	0.69	0.59	0.69	0.69	0.60	0.68	0.67	0.67	0.72	0.65	0.70	0.66	0.74	0.67	0.65	0.68	0.70

Na	0.31	0.37	0.31	0.32	0.35	0.31	0.31	0.34	0.28	0.36	0.30	0.34	0.26	0.32	0.33	0.34	0.29
K	0.00	0.02	0.00	0.00	0.04	0.00	0.01	0.00	0.01	0.00	0.00	0.00	0.00	0.01	0.01	0.01	0.01
Cl	0.00	0.00	0.00	0.00	0.00	0.00	0.00	0.00	0.00	0.00	0.00	0.00	0.00	0.00	0.00	0.00	0.00
F	0.03	0.00	0.01	0.00	0.00	0.01	0.01	0.00	0.01	0.00	0.00	0.00	0.00	0.02	0.00	0.02	0.02
Ba	0.00	0.01	0.00	0.00	0.00	0.00	0.01	0.01	0.00	0.00	0.00	0.00	0.00	0.00	0.00	0.00	0.00
Total	5.02	4.99	5.01	5.00	5.01	5.00	5.00	5.01	5.01	5.01	4.99	5.00	5.00	5.02	5.00	5.05	5.01
An(%)	69.02	59.89	68.45	68.11	60.66	68.52	67.75	66.24	71.77	64.47	70.06	66.02	73.56	67.00	65.61	66.12	70.41
Ab(%)	30.62	37.69	31.21	31.70	35.77	31.18	31.58	33.47	27.70	35.16	29.49	33.52	26.22	32.24	33.41	33.27	29.06
Or(%)	0.36	2.41	0.34	0.18	3.58	0.30	0.67	0.29	0.53	0.36	0.45	0.47	0.22	0.77	0.98	0.61	0.53

Grain 2																	
Location	**Core**																**Rim**
SiO_2	50.39	50.59	50.73	50.75	50.77	51.18	50.15	50.77	50.99	50.27	52.17	50.40	52.23	51.70	51.59	51.64	51.92
TiO_2	0.03	0.07	0.03	0.03	0.00	0.05	0.08	0.00	0.00	0.00	0.00	0.00	0.00	0.07	0.00	0.00	0.16
Al_2O_3	31.15	31.04	31.12	31.14	31.28	31.27	31.17	31.20	30.93	31.15	30.08	31.55	30.01	30.28	31.10	30.44	30.12
FeO	0.41	0.32	0.29	0.42	0.34	0.43	0.25	0.29	0.29	0.24	0.22	0.34	0.23	0.36	0.35	0.42	0.48
MnO	0.00	0.00	0.00	0.00	0.00	0.00	0.00	0.03	0.02	0.04	0.02	0.02	0.00	0.00	0.00	0.07	0.05
MgO	0.00	0.00	0.00	0.00	0.00	0.00	0.00	0.00	0.00	0.00	0.00	0.00	0.00	0.00	0.00	0.00	0.00
CaO	14.54	14.64	14.73	14.92	14.50	14.64	14.38	14.43	14.30	14.29	14.12	14.98	13.54	13.76	14.54	13.94	13.58
Na_2O	3.41	3.22	3.13	3.32	3.27	3.36	3.42	3.34	3.42	3.37	3.28	3.03	3.92	3.85	3.37	3.55	3.84
K_2O	0.12	0.07	0.05	0.04	0.04	0.07	0.06	0.04	0.06	0.09	0.09	0.04	0.09	0.05	0.10	0.08	0.09
Cl	0.00	0.01	0.02	0.00	0.00	0.00	0.00	0.00	0.01	0.01	0.00	0.00	0.00	0.00	0.01	0.01	0.00
F	0.05	0.00	0.00	0.00	0.00	0.00	0.00	0.17	0.00	0.10	0.00	0.35	0.20	0.00	0.08	0.00	0.01
BaO	0.00	0.00	0.13	0.00	0.00	0.38	0.02	0.32	0.04	0.00	0.00	0.01	0.10	0.00	0.00	0.04	0.00
Total	100.10	99.98	100.22	100.61	100.21	101.39	99.53	100.59	100.06	99.56	99.97	100.71	100.32	100.07	101.14	100.19	100.25

Calculation based on 8 O																	
Si	2.30	2.31	2.31	2.30	2.31	2.31	2.30	2.30	2.32	2.30	2.37	2.28	2.36	2.35	2.32	2.35	2.36
Ti	0.00	0.00	0.00	0.00	0.00	0.00	0.00	0.00	0.00	0.00	0.00	0.00	0.00	0.00	0.00	0.00	0.01
Al	1.67	1.67	1.67	1.67	1.68	1.66	1.68	1.67	1.66	1.68	1.61	1.68	1.60	1.62	1.65	1.63	1.61
Fe	0.02	0.01	0.01	0.02	0.01	0.02	0.01	0.01	0.01	0.01	0.01	0.01	0.01	0.01	0.01	0.02	0.02
Mn	0.00	0.00	0.00	0.00	0.00	0.00	0.00	0.00	0.00	0.00	0.00	0.00	0.00	0.00	0.00	0.00	0.00
Mg	0.00	0.00	0.00	0.00	0.00	0.00	0.00	0.00	0.00	0.00	0.00	0.00	0.00	0.00	0.00	0.00	0.00
Ca	0.71	0.72	0.72	0.73	0.71	0.71	0.71	0.70	0.70	0.70	0.69	0.73	0.66	0.67	0.70	0.68	0.66
Na	0.30	0.29	0.28	0.29	0.29	0.29	0.30	0.29	0.30	0.30	0.29	0.27	0.34	0.34	0.29	0.31	0.34
K	0.01	0.00	0.00	0.00	0.00	0.00	0.00	0.00	0.00	0.01	0.01	0.00	0.01	0.00	0.01	0.00	0.01
Cl	0.00	0.00	0.00	0.00	0.00	0.00	0.00	0.00	0.00	0.00	0.00	0.00	0.00	0.00	0.00	0.00	0.00
F	0.01	0.00	0.00	0.00	0.00	0.00	0.00	0.02	0.00	0.01	0.00	0.05	0.03	0.00	0.01	0.00	0.00
Ba	0.00	0.00	0.00	0.00	0.00	0.01	0.00	0.01	0.00	0.00	0.00	0.00	0.00	0.00	0.00	0.00	0.00
Total	5.02	5.00	4.99	5.01	5.00	5.01	5.01	5.01	5.00	5.01	4.97	5.02	5.01	5.00	5.00	4.99	5.00
An(%)	69.76	71.21	72.00	71.11	70.84	70.34	69.69	70.33	69.55	69.73	70.04	73.02	65.31	66.19	70.03	68.13	65.79
Ab(%)	29.57	28.37	27.72	28.65	28.93	29.23	29.94	29.46	30.09	29.77	29.41	26.76	34.17	33.53	29.40	31.41	33.67
Or(%)	0.67	0.43	0.27	0.24	0.23	0.42	0.37	0.21	0.36	0.50	0.54	0.22	0.52	0.29	0.57	0.45	0.54

Grain 3																				
Location	**Core**																			**Rim**
SiO_2	51.21	51.12	51.08	50.59	51.11	51.67	51.69	50.84	51.37	51.83	51.59	51.65	52.02	52.28	52.25	51.58	51.14	49.92	51.77	52.25
TiO_2	0.12	0.02	0.00	0.00	0.12	0.00	0.03	0.16	0.00	0.10	0.00	0.10	0.10	0.00	0.04	0.00	0.00	0.00	0.00	0.00
Al_2O_3	31.39	30.73	30.82	30.44	30.96	30.92	31.02	30.62	30.79	30.74	30.64	30.04	30.51	30.70	30.33	30.70	30.67	31.41	30.41	29.90
FeO	0.38	0.31	0.33	0.45	0.31	0.52	0.43	0.33	0.30	0.17	0.40	0.34	0.28	0.25	0.20	0.36	0.38	0.25	0.22	0.21
MnO	0.02	0.00	0.06	0.00	0.00	0.00	0.00	0.00	0.00	0.00	0.06	0.00	0.03	0.00	0.00	0.05	0.00	0.01	0.00	0.01

MgO	0.00	0.00	0.00	0.00	0.00	0.00	0.00	0.00	0.00	0.00	0.00	0.00	0.00	0.00	0.00	0.00	0.00	0.00	0.00	0.00
CaO	14.28	14.46	14.45	14.34	14.16	14.23	14.00	14.11	14.26	14.05	13.88	13.92	13.65	13.53	13.47	13.96	13.95	14.77	13.97	13.49
Na_2O	3.25	3.71	3.54	3.30	3.48	3.50	3.63	3.53	3.67	3.49	3.64	3.58	3.66	3.90	4.18	3.67	3.63	3.26	3.41	3.74
K_2O	0.05	0.05	0.11	0.11	0.06	0.09	0.14	0.18	0.23	0.22	0.19	0.19	0.10	0.06	0.06	0.06	0.13	0.06	0.07	0.05
Cl	0.00	0.01	0.00	0.00	0.00	0.00	0.00	0.02	0.00	0.00	0.00	0.00	0.01	0.01	0.00	0.00	0.02	0.03	0.02	0.01
F	0.10	0.00	0.08	0.07	0.00	0.14	0.07	0.24	0.02	0.07	0.00	0.23	0.00	0.14	0.00	0.07	0.00	0.01	0.14	0.00
BaO	0.07	0.00	0.00	0.00	0.00	0.00	0.29	0.00	0.35	0.07	0.04	0.00	0.00	0.00	0.04	0.19	0.10	0.00	0.06	0.00
Total	100.86	100.40	100.56	99.36	100.29	101.07	101.35	100.02	101.02	100.77	100.47	100.13	100.38	100.86	100.57	100.64	100.04	99.70	100.09	99.69
Calculation based on 8 O																				
Si	2.31	2.32	2.32	2.32	2.32	2.33	2.33	2.31	2.33	2.34	2.34	2.35	2.36	2.35	2.36	2.34	2.33	2.29	2.35	2.38
Ti	0.00	0.00	0.00	0.00	0.00	0.00	0.00	0.01	0.00	0.00	0.00	0.00	0.00	0.00	0.00	0.00	0.00	0.00	0.00	0.00
Al	1.67	1.65	1.65	1.65	1.66	1.64	1.65	1.64	1.64	1.64	1.64	1.61	1.63	1.63	1.62	1.64	1.65	1.70	1.63	1.60
Fe	0.01	0.01	0.01	0.02	0.01	0.02	0.02	0.01	0.01	0.01	0.02	0.01	0.01	0.01	0.01	0.01	0.01	0.01	0.01	0.01
Mn	0.00	0.00	0.00	0.00	0.00	0.00	0.00	0.00	0.00	0.00	0.00	0.00	0.00	0.00	0.00	0.00	0.00	0.00	0.00	0.00
Mg	0.00	0.00	0.00	0.00	0.00	0.00	0.00	0.00	0.00	0.00	0.00	0.00	0.00	0.00	0.00	0.00	0.00	0.00	0.00	0.00
Ca	0.69	0.70	0.70	0.71	0.69	0.69	0.68	0.69	0.69	0.68	0.68	0.68	0.66	0.65	0.65	0.68	0.68	0.72	0.68	0.66
Na	0.28	0.33	0.31	0.29	0.31	0.31	0.32	0.31	0.32	0.31	0.32	0.32	0.32	0.34	0.37	0.32	0.32	0.29	0.30	0.33
K	0.00	0.00	0.01	0.01	0.00	0.01	0.01	0.01	0.01	0.01	0.01	0.01	0.01	0.00	0.00	0.00	0.01	0.00	0.00	0.00
Cl	0.00	0.00	0.00	0.00	0.00	0.00	0.00	0.00	0.00	0.00	0.00	0.00	0.00	0.00	0.00	0.00	0.00	0.00	0.00	0.00
F	0.01	0.00	0.01	0.01	0.00	0.02	0.01	0.03	0.00	0.01	0.00	0.03	0.00	0.02	0.00	0.01	0.00	0.00	0.02	0.00
Ba	0.00	0.00	0.00	0.00	0.00	0.00	0.01	0.00	0.01	0.00	0.00	0.00	0.00	0.00	0.00	0.00	0.00	0.00	0.00	0.00
Total	4.99	5.02	5.01	5.00	5.00	5.01	5.01	5.02	5.02	5.00	5.00	5.01	4.99	5.01	5.01	5.01	5.01	5.01	4.99	4.98
An(%)	70.66	68.10	68.87	70.12	68.96	68.85	67.50	68.17	67.38	68.13	67.10	67.45	66.95	65.53	63.85	67.53	67.53	71.23	69.08	66.39
Ab(%)	29.08	31.60	30.51	29.23	30.69	30.65	31.72	30.81	31.34	30.61	31.80	31.43	32.45	34.14	35.83	32.14	31.75	28.45	30.50	33.32
Or(%)	0.27	0.30	0.62	0.65	0.35	0.51	0.79	1.01	1.28	1.26	1.09	1.12	0.60	0.33	0.32	0.33	0.72	0.32	0.42	0.29

mafic- and felsic magmas cannot be traced. Petrographic- and geochemical signatures have shown that the porphyritic intermediate rock formed by the mixing of parental end-member magmas (Gogoi et al. 2018b). The homogenous nature of the rock suggests the uniform mixing of the mafic- and felsic magmas. A detailed overview on magma mixing and mingling in the GFD is presented in Gogoi et al. (2018b).

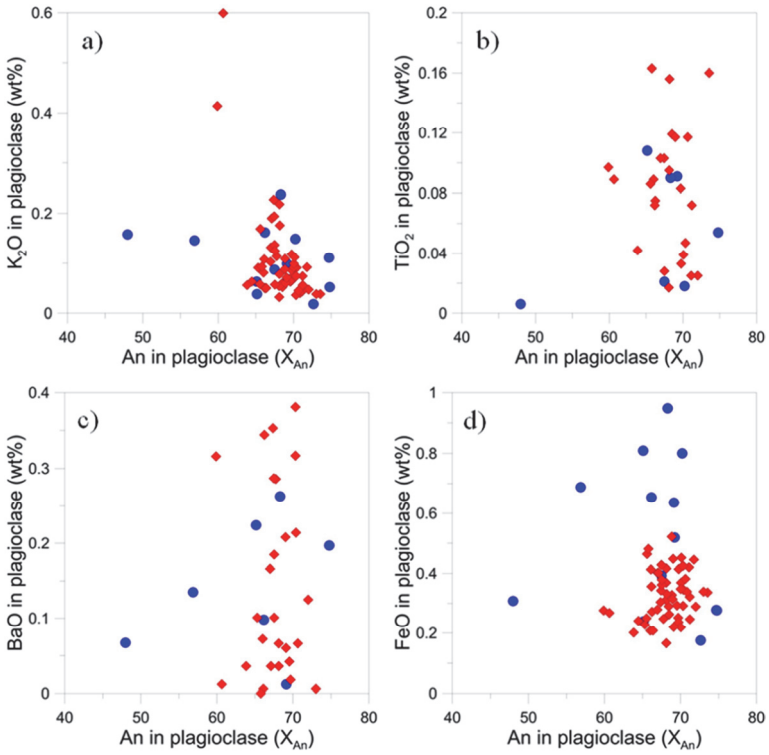

Fig. 6. Plagioclase composition from the mafic and porphyritic intermediate rocks showing the variation of K_2O, TiO_2, BaO and FeO as a function of anorthite content. Symbols represent: blue circle = plagioclase composition from the mafic end-member; red diamond = plagioclase composition from the porphyritic intermediate rock.

A detailed study of the porphyritic intermediate rock under the microscopic reveals that smaller crystals of plagioclase have aggregated together to form larger crystal clusters or phenocrysts. The crystals involved in the clusters are mutually attached along prominent euhedral crystal faces (Fig. 4c and e). Glomerocrysts with crystals attached along prominent euhedral crystal faces form by synneusis as the mineral is crystallizing (Hogan 1993). Petrographic- observations suggest that plagioclase-crystal aggregation was followed by dissolution of their grain boundaries to form phenocrysts of plagioclase. The degree of coalescence between the plagioclase grains involved in synneusis varies significantly. In some cases, the crystals show aggregation with their grain boundaries intact (Fig. 4c) whereas, in others, complete dissolution of grain boundaries results in larger plagioclase grains (Fig. 4d and f). The nature of the grain boundaries can point to the

degree of synneusis undergone. Glomerocrysts in which grain boundaries of the individual crystals are preserved show distinct extinction positions but behave as single crystals with regard to sericitization or alteration patterns (Fig. 4c). On the other hand, crystal clusters characterized by dissolved grain boundaries formed optically continuous glomerocrysts which subsequently evolved into single plagioclase grains.

The plagioclase from both the mafic- and porphyritic intermediate rocks mostly plot in the fields of labradorite and bytownite (Fig. 5a and b). The plagioclase of the mafic rocks varies from An_{48}-An_{68} in the cores to An_{65}-An_{73} in the rims (Table 1); the plagioclase exhibits reverse zoning. The crystals involved in synneusis in the porphyritic intermediate rock have compositions ranging from $An_{69\text{-}71}$ in the cores to $An_{66\text{-}70}$ in the rims (Table 2). The plagioclases of the crystal clusters are characterized by restricted compositional ranges and do not exhibit any definite zoning pattern. The compositional similarity between the plagioclase from the mafic rocks and the glomerocrysts of the porphyritic intermediate rock suggests that the plagioclase occurring in the hybrid rock may have been derived from the mafic magma.

A significant portion of the GFD is occupied by mafic rocks containing clasts and ocelli of the felsic host rocks. From field observations, it is inferred that the felsic magma chamber was partly solidified when mafic magma intruded. The solidified portion of the magma chamber is now represented by the clasts and ocelli in the mafic rocks. The melt in the remaining portion of the chamber interacted with the mafic magma to form hybrid rocks. Among the hybrid rocks, a porphyritic grey-colored intermediate rock occurs which is characterized by abundant phenocrysts of plagioclase feldspar arranged in glomerocrysts or crystal clusters. The clustered plagioclase crystals are joined along prominent euhedral crystal faces suggesting that the glomerocrysts formed by synneusis. The preservation of synneusis in the hybrid rock suggests that crystals drifting in a melt mutually attached together to form phenocrysts. The similar compositions of the plagioclase in the mafic- and porphyritic intermediate rocks suggest that the plagioclase in the hybrid rock derived from the mafic magma. From the porphyritic- and coarse-grained nature of the mafic rocks, it is inferred that the mafic magma was crystal-rich when it intruded. On intrusion, crystals from the mafic magma were dispersed into the crystal-poor felsic melt from which the fine-grained felsic rocks evolved. The crystal-poor nature of the felsic melt allowed the plagioclase crystals of the mafic end-member to drift and accumulate together to form larger crystals in an intermediate hybrid rock of porphyritic nature (Dowty 1982; Stull 1979; Vance 1969)

There are several hypotheses suggesting the role of crystal mushes in the origin of crystal clusters (Murata, Richter 1966; Schwindinger, Anderson 1989; Jerram et al. 2003). Crystal aggregates could be entrained by the vertical influx of magma through a cumulate mush or the reworking of crystal mushes from the walls and roof of a magma chamber. However, the absence of cumulate layers in the Ghansura dome suggests that mush zones were not responsible for the origin of the crystal clusters in the porphyritic intermediate rock. From field observations, it appears that the GFD was partly solid and partly melt when mafic magma intruded. The solidified portion of the felsic magma chamber is now represented by clasts and ocelli in the mafic rocks. The clasts and ocelli are fine-grained rocks resembling the felsic host. On the other hand, the felsic melt interacted with the intruding mafic magma to form the porphyritic intermediate rock. Evidence for the

existence of a crystal-rich mush zone in the GFD was not found. Mush zones have frequently been associated with felsic magma chambers from both plutonic and volcanic settings (Hildreth, Wilson 2007; Bachmann, Bergantz 2008; Takahashi, Nakagawa 2012; Singer et al. 2014). The lack of mush zones in the GFD may be attributed to the shallow depth of the felsic magma chamber where fast cooling rates might well have prevented the formation of crystal-rich mushes in the felsic magma. Thus, felsic magma chambers may behave differently under different physical conditions.

8. Conclusions

Here we report the occurrence of synneusis in a porphyritic intermediate rock. Synneusis is displayed by smaller plagioclase crystals that have aggregated and mutually attached to form larger crystals or phenocrysts. Thus, synneusis is responsible for the formation of plagioclase phenocrysts occurring in the hybrid rock and giving the rock its characteristic porphyritic nature. Textural- and mineral chemical analyses suggest that the synneusis texture resulted from the mixing of a crystal-rich mafic magma with a crystal-poor felsic melt. Earlier studies have mainly suggested the genesis of synneusis as due to crystal settling in a magma chamber. Our study suggests that synneusis may be an important mechanism in the formation of porphyritic rocks. Furthermore, the nature of the interaction observed between the invading mafic magma and the felsic host in the Ghansura dome indicates that shallow-level crustal magma chambers may be partly solidified and partly melt (crystal-poor) when undergoing cooling. Our study of synneusis illustrates how the mixing of a crystal-rich mafic magma and a crystal-poor felsic melt can lead to the development of this unique texture.

Acknowledgements. Ashima Saikia acknowledges a CSIR grant vide Project no. 24(0317)/12/EMR-II. Bibhuti Gogoi acknowledges a CSIR JRF/SRF fellowship no. 09/045(1146)/2011-EMR1. Reviewers A. K. Barker, Ulf B. Andersson, Jarosław Majka and Marek Michalik are warmly acknowledged for their constructive reviews.

9. References

Acharyya, S.K. (2003). The nature of Mesoproterozoic central Indian tectonic zone with exhumed and reworked older granulites. *Gondwana Research, 6*, 197-214. DOI: 10.1016/S1342-937X(05)70970-9.

Ahmad, M., & Paul, A.Q. (2013). Investigation of Volcano-Sedimentary Sequence and Associated Rocks to Identify Gold and Base Metal Mineralization at Gere-Kewti Area of Gaya District, Bihar (G4). *Unpublished Report Geological Society of India, Bangalore*.

Bachmann, O., & Bergantz, G.W. (2004). On the origin of crystal-poor rhyolites: extracted from batholithic crystal mushes. *Journal of Petrology, 45*, 1565-1582. DOI: 10.1093/petrology/egh019.

Baxter, S., & Feely, M. (2002). Magma mixing and mingling textures in granitoids: examples from the Galway Granite, Connemara, Ireland. *Mineralogy and Petrology, 76*, 63-74. DOI: 10.1007/s007100200032.

Brothers, R.N. (1964). Petrofabric analyses of Rhum and Skaergaard layered rocks. *Journal of Petrology, 6*, 255-274. DOI: 10.1093/petrology/5.2.255.

Brown, G.M. (1956). The layered ultrabasic rocks of Rhum, Inner Hebrides. *Philosophical Transactions of the Royal Society London, Ser. B, 240*, 1-53. DOI: 10.1098/rstb.1956.0011.

Castro, A., De la Rosa, J.D., & Stephens, W.E. (1990). Magma mixing in the subvolcanic environment: petrology of the Gerena interaction zone near Seville, Spain. *Contributions to Mineralogy and Petrology, 105*, 9-26. DOI: 10.1007/BF00306405.

Charreteur, G., & Tegner, C. (2013). Magmatic emulsion texture formed by mixing during extrusion, Raudafell composite complex, Breiddalur volcano, eastern Iceland. *Bulletin of Volcanology, 75*, 721. DOI: 10.1007/s00445-013-0721-6.

Chatterjee, N., & Ghosh, N.C. (2011). Extensive early neoproterozoic highgrade metamorphism in North Chotanagpur Gneissic Complex of the central Indian tectonic zone. *Gondwana Research*, 20, 362-379. DOI: 10.1016/j.gr.2010.12.003.

Clague, D.A., Moore, J.G., Dixon, J.E., & Friesen, W.B. (1995). Petrology of submarine lavas from Kilaueas Puna Ridge, Hawaii. *Journal of Petrology, 36*, 299-349. DOI: 10.1093/petrology/36.2.299.

DePaolo, D.J. (1981). Trace-element and isotopic effects of combined wallrock assimilation and fractional crystallization. *Earth and Planetary Science Letters, 53*, 189-202. DOI: 10.1016/0012-821X(81)90153-9.

Dowty, E. (1980). Synneusis reconsidered. *Contributions to Mineralogy and Petrology, 74*, 75-84. DOI: 10.1007/BF00375491.

Eichelberger, J.C. (1975). Origin of andesite and dacite; evidence of magma mixing at Glass Mountain in California and the other Circum-Pacific volcanoes. *Geological Society of America Bulletin, 86*, 1381-1391. DOI: 10.1130/0016-7606(1975)86<1381:OOAADE>2.0.CO;2.

Faure, G. (1986). *Principles of Isotope Geology*. Chichester: J. Wiley & Sons.

Gogoi, B., Saikia, A., & Ahmad, M. (2017). Titanite-centered ocellar texture: A petrological tool to unravel the mechanism enhancing magma mixing. *Periodico di Mineralogia, 86*, 245-273.

Gogoi, B., Saikia, A., & Ahmad, M. (2018a) Field evidence, mineral chemical and geochemical constraints on mafic-felsic magma interactions in a vertically zoned magma chamber from the Chotanagpur Granite Gneiss Complex of Eastern India. *Chemie der Erde, 78(1)*, 78-102. DOI: 10.1016/j.chemer.2017.11.003.

Gogoi, B., Saikia, A., Ahmad, M., & Ahmad, T. (2018b). Evaluation of magma mixing in the subvolcanic rocks of Ghansura Felsic Dome of Chotanagpur Granite Gneiss Complex, eastern India. *Mineralogy and Petrology, 112*, 393-413. DOI: 10.1007/s00710-017-0540-0.

Gogoi, B. & Saikia, A. (2018). Role of viscous folding in magma mixing. *Chemical Geology*, *501*, 26-34. DOI: 10.1016/j.chemgeo.2018.09.035.

Grove, T.L., Kinzler, R.J., Baker, M.B., Donelly-Nollan, J.M. & Lesher, C.E. (1988). Assimilation of granite by basaltic magma at Burnt Lava Flow, Medicine Lake Volcano, Northern California, decoupling of heat and mass-transfer. *Contributions to Mineralogy and Petrology, 99*, 320-343.

Hawkesworth, C.J., Blake, S., Evans, P., Hughes, R., Macdonald, R., Thomas, L.E., Turner, S.P., & Zellmer, G. (2000). Time scales of crystal fractionation in magma chambers. Integrating physical, isotopic and geochemical perspectives. *Journal of Petrology, 41*, 991-1006. DOI: 10.1093/petrology/41.7.991.

Hibbard, M.J. (1991). Textural anatomy of twelve magma-mixed granitoid systems. In J. Didier & B. Barbarin (Eds.) Enclaves and granite petrology (pp. 431-444). Elsevier, Amsterdam.

Hildreth, W., & Wilson, C.J.N. (2007). Compositional zoning of the Bishop Tuff. *Journal of Petrology, 48*, 951-999. DOI: 10.1093/petrology/egm007.

Hogan, J.P. (1993). Monomineralic Glomerocrysts: Textural Evidence for Mineral Resorption During Crystallization of Igneous Rocks. *The Journal of Geology, 101*, 531-540.

Huppert, H.E., Turner, J.S., Stephen, R., & Sparks, J. (1982). Replenished magma chambers; effects of compositional zonation and input rates. *Earth and Planetary Science Letters, 57*, 345-357. DOI: 10.1016/0012-821X(82)90155-8.

Ikeda, S., Toriumi, M., Yoshida, H., & Shimizu, I. (2002). Experimental study of the textural development of igneous rocks in the late stage of crystallization: the importance of interfacial energies under non-equilibrium conditions. *Contributions to Mineralogy and Petrology, 142*, 397-415. DOI: 10.1007/s004100100300.

Jerram, D.A., Cheadle, M.J., & Philpotts, A.R. (2003). Quantifying the Building Blocks of Igneous Rocks: Are Clustered Crystal Frameworks the Foundation? *Journal of Petrology, 44*, 2033-2051. DOI: 10.1093/petrology/egg069.

Koyaguchi, T. (1986). Textural and compositional evidence for magma mixing and its mechanism, Abu volcano group, Southwestern Japan. *Contributions to Mineralogy and Petrology, 93*, 33-45. DOI: 10.1007/BF00963583.

Larsen, E.S., Irving, J., Gonyer, F., & Larsen, E.S.III. (1938). Petrologic results of study of the minerals from the Tertiary volcanic rocks of the San Juan region, Colorado. *American Mineralogist, 23*, 227-257.

Luhr, J.F., & Carmichael, I.S.E. (1980). The Colima volcanic complex, Mexico, I. Post caldera andesites from Volcan Colima. *Contributions to Mineralogy and Petrology, 71*, 343-372. DOI: 10.1007/BF00374707.

Marsh, B.D. (1998). On the interpretation of crystal size distributions in magmatic systems. *Journal of Petrology, 39*, 553-599. DOI: 10.1093/petroj/39.4.553.

Martin, V.M., Holness, M.B., & Pyle, D.M. (2006). Textural analysis of magmatic enclaves from the Kameni Islands, Santorini, Greece. *Journal of Volcanology and Geothermal Research, 154*, 89-102. DOI: 10.1016/j.jvolgeores.2005.09.021.

Murata, K. J., & Richter, D. H. (1966). The settling of olivine in Kilauean magma as shown by lavas of the 1959 eruption. *American Journal of Science, 264*, 194-203. DOI: 10.2475/ajs.264.3.194.

Perugini, D., Poli, G., Christofides, G., & Eleftheriadis, G. (2003). Magma mixing in the Sithonia Plutonic Complex, Greece: evidence from mafic microgranular enclaves. *Mineralogy and Petrology, 78*(3-4), 173-200. DOI: 10.1007/s00710-002-0225-0.

Pietranik, A., & Koepke, J. (2009). Interactions between dioritic and granodioritic magmas in mingling zones: plagioclase record of mixing, mingling and subsolidus interactions in the Gęsiniec Intrusion, NE Bohemian Massif, SW Poland. *Contributions to Mineralogy and Petrology, 158*, 17-36. DOI: 10.1007/s00410-008-0368-z.

Pouchou, J.L., & Pichoir, F. (1987). Basic expressions of PAP computation for quantitative EPMA. *Proceedings of ICXOM 11, Ontario*, 249-253.

Renjith, M.L. (2014). Micro-textures in plagioclase from 1994-1995 eruption, Barren Island Volcano: Evidence of dynamic magma plumbing system in the Andaman subduction zone. *Geoscience Frontiers, 5*, 113-126. DOI: 10.1016/j.gsf.2013.03.006.

Renjith, M.L., Charan, S.N., Subbarao, D.V., Babu, E.V.S.S.K., & Rajashekhar, V.B. (2014). Grain to outcrop-scale frozen moments of dynamic magma mixing in the syenite magma chamber, Yelagiri Alkaline Complex, South India. *Geoscience Frontiers*, 5, 801-820. DOI: 10.1016/j.gsf.2013.08.006.

Saikia, A., Gogoi, B., Ahmad, M., & Ahmad, T. (2014). Geochemical constraints on the evolution of mafic and felsic rocks in the Bathani volcano-sedimentary sequence of Chotanagpur Granite Gneiss Complex. *Journal of Earth System Science, 123(5)*, 959-987. DOI: 10.1007/s12040-014-0455-7.

Sakuyama, M. (1981). Petrological study of the Myoko and Kurohime volcanoes, Japan: Crystallization sequence and evidence for magma mixing. *Journal of Petrology, 22*, 553-583. DOI: 10.1093/petrology/22.4.553.

Schwindinger, K.R. (1999). Particle dynamics and aggregation of crystals in a magma chamber with application to Kilauea Iki olivines. *Journal of Volcanology and Geothermal Research, 88*, 209-238. DOI: 10.1016/S0377-0273(99)00009-8.

Schwindinger, K.R., & Anderson, A.T. Jr. (1989). Synneusis of Kilauea Iki olivines. *Contributions to Mineralogy and Petrology, 103*, 187-198. DOI: 10.1007/BF00378504.

Singer, B.S., Andersen, N.L., Le Mével, H. & others (2014). Dynamics of a large, restless, rhyolitic magma system at Laguna del Maule, southern Andes, Chile. *GSA Today, 24*, 4-10. DOI: 10.1130/GSATG216A.1.

Sosa-Ceballos, G., Gardner, J.E., Siebe, C., & Macías, J.L. (2012). A caldera-forming eruption 14,100 ^{14}C yr BP at Popocatépetl volcano, México: Insights from eruption dynamics and magma mixing. *Journal of Volcanology and Geothermal Research, 213-214*, 27-40. DOI: 10.1016/j.jvolgeores.2011.11.001.

Sparks, R.S., Sigurdsson, H., & Wilson, L. (1977). Magma mixing: a mechanism for triggering acid explosive eruptions. *Nature, 267*, 315-317. DOI: 10.1038/267315a0.

Stull, R.J. (1979). Mantled feldspars and synneusis. *American Mineralogist, 64*, 514-518.

Takahashi, R., & Nakagawa M. (2012). Formation of a Compositionally Reverse Zoned Magma Chamber: Petrology of the AD 1640 and 1694 Eruptions of Hokkaido-Komagatake Volcano, Japan. *Journal of Petrology, 54*, 815-838. DOI: 10.1093/petrology/egs087.

Vance, J.A. (1969). On synneusis. *Contributions to Mineralogy and Petrology, 24*, 7-29. DOI: 10.1007/BF00398750.

Vernon, R.H., Etheridge, M.A., & Wall, V.J. (1988). Shape and microstructure of microgranitoid enclaves: indicators of magma mingling and flow. *Lithos, 22*, 1-11.

Vogt, J.H.L. (1921). The physical chemistry of the crystallization and magmatic differentiation of igneous rocks. *Journal of Geology, 28*, 318-350.